DOI: 10.1002/chem.200701949

$Li_2B_{12}Si_2$: The First Ternary Compound in the System Li/B/Si: Synthesis, Crystal Structure, Hardness, Spectroscopic Investigations, and Electronic Structure

Natascha Vojteer, Melanie Schroeder, Caroline Röhr, and Harald Hillebrecht*[a]

Abstract: We present the synthesis, crystal structure, hardness, IR/Raman and UV/Vis spectra, and FP-LAPW calculations of the electronic structure of $Li_2B_{12}Si_2$, the first ternary compound in the system Li/B/Si. Yellow, transparent single crystals were synthesized from the elements in tin as solvent at 1500 °C in h-BN crucibles in arc-welded Ta ampoules. $Li_2B_{12}Si_2$ crystallizes orthorhombic in the space group *Cmce* (no. 64) with $a=6.1060(6)$, $b=10.9794(14)$, $c=8.4050(8)$ Å, and $Z=4$. The crystal structure is characterized by a covalent network of B_{12} icosahedra connected by Si atoms and Li atoms located in interstitial spaces. The structure is closely related to that of $MgB_{12}Si_2$ and fulfils the electron-counting rules of Wade and Longuet-Higgins. Measurements of Vickers ($H_V=20.3$ GPa) and Knoop microhardness ($H_K=20.4$ GPa) revealed that $Li_2B_{12}Si_2$ is a hard material. The band gap was determined experimentally and calculated by theoretical means. UV/Vis spectra revealed a band gap of 2.27 eV, with which the calculated value of 2.1 eV agrees well. The IR and Raman spectra show the expected oscillations of icosahedral networks. Theoretical investigations of bonding in this structure were carried out with the FP-LAPW method. The results confirm the applicability of simple electron-counting rules and enable some structural specialties to be explained in more detail.

Keywords: boron · electronic structure · lithium · silicon · solid-state structures

Introduction

Boron-rich borides are a class of compounds that is of particular interest to solid-state chemistry. The one-of-a-kind structural chemistry of elemental boron is strongly influenced by impurities, and thus systematic insertion of other elements often causes characteristic structural changes in the framework of boron polyhedra and leads to the formation of a variety of different crystal structures in the class of boron-rich borides.[1] These compounds are of interest in materials science because their mechanical and electronic properties give rise to several high-temperature (HT) applications, for example, as HT semiconductors[2] and HT thermoelectrics.[3] Furthermore, the refractory nature of these materials makes them applicable as abrasives[4] and components of composites.[5] In addition, the special electronic structure of boron-rich borides is a topic of current research.[6] Band-structure calculations on this class of compounds are quite difficult and hard to interpret, as the crystal structures consist of complicated covalent 3D networks dominated by boron polyhedra, and they have large unit cells. Moreover, compositions are often nonstoichiometric and the crystals or powders are mostly black. However, when the first colorless and electron-precise boron-rich borides were synthesized,[7,8] interest in band-structure calculations on these compounds was aroused,[6] as there are reasons to believe that the results will be meaningful for the comprehension of bonding in networks of boron polyhedra. The crystal structures of these compounds—$Li_2B_{12}C_2$, $LiB_{13}C_2$, and $MgB_{12}Si_2$—are remarkably simple. Their compositions are stoichiometric with every atom position fully occupied.[7,8] Therefore, the rules of Wade and Longuet-Higgins are fulfilled: every B_{12} icosahedron requires two electrons, which are provided by the metal atoms.[9] This assignment of electrons is confirmed by the fact that the single crystals are almost colorless.

Using the well-established method of dispersing and dissolving the elements in molten metals in boron nitride crucibles welded into Ta ampoules,[10–12] we were able to synthesize another electron-precise compound of this family, namely, $Li_2B_{12}Si_2$, the first ternary compound of the Li/B/Si

[a] Dipl.-Chem. N. Vojteer, Dipl.-Chem. M. Schroeder, Prof. Dr. C. Röhr, Prof. Dr. H. Hillebrecht
Institut für Anorganische und Analytische Chemie
Albertstrasse 21, 79104 Freiburg (Germany)
Fax: (+49) 761-203-6021
E-mail: harald.hillebrecht@ac.uni-freiburg.de

system. The crystal structure was solved and refined on the basis of single-crystal data. It is closely related to that of $MgB_{12}Si_2$.[8] The composition was confirmed by wavelength- and energy-dispersive X-ray (WDX and EDX) measurements. We also determined the hardness of $Li_2B_{12}Si_2$. The band gap, measured by means of UV/VIS spectroscopy, supports the calculated value. IR and Raman spectra were taken and discussed. We also calculated the band structure of $Li_2B_{12}Si_2$ (FP-LAPW method), and the results match the experimentally observed properties of the single crystals well.

Results and Discussion

Description of the structure: Single crystals of $Li_2B_{12}Si_2$ are yellow and transparent (Figure 1) and their composition is

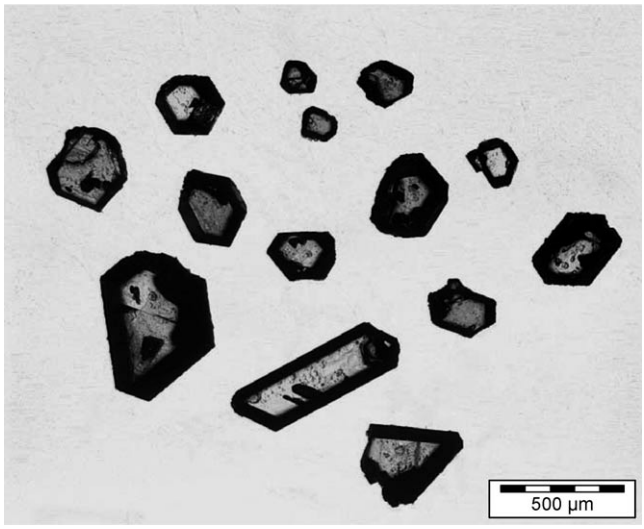

Figure 1. Single crystals of $Li_2B_{12}Si_2$.

stoichiometric, just like the lithium boride carbides and the magnesium boride silicide mentioned above.[7,8] The sum formula can be written according to the rules of Wade and Longuet-Higgins[9] as $(Li^+)_2(B_{12}^{2-})(Si)_2$ or $(Li^+)_2(B_{12}Si_2^{2-})$; hence the covalent framework is anionic, made up of B_{12}^{2-} icosahedra and neutral Si atoms; Li ions occupy voids of the framework.

The icosahedra are arranged in nearly hexagonal layers that are stacked along [010] in an ABAB sequence. Li and Si atoms are located between the layers, which the Si atoms interconnect to form a covalent 3D framework (Figure 2). Each B_{12}^{2-} unit is linked to four other icosahedra by four exohedral B–B bonds (B4–B4 1.795(2) Å) within the layer and has eight exohedral B–Si bonds (2.015(1)–2.070(1) Å), four above and four below the layer (Figure 3). The connection of B_{12} icosahedra by four exohedral B–B bonds into almost hexagonal layers is discovered frequently in boron-rich borides, for example, in the lithium boride carbides[7] MgB_7,[13] $MgB_{12}C_2$,[10d,e,11] $Mg_3B_{50}C_8$[10e] and $MgB_{12}Si_2$.[8]

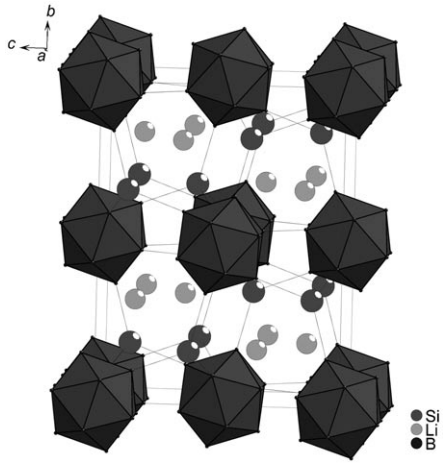

Figure 2. Crystal structure of $Li_2B_{12}Si_2$.

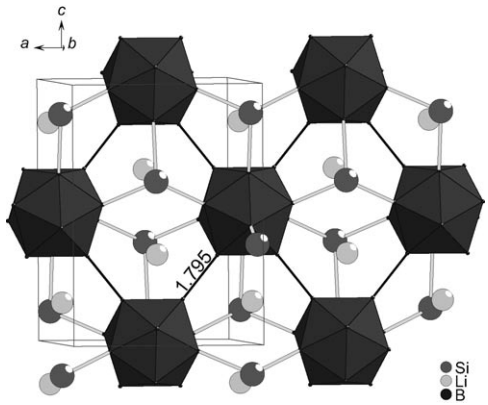

Figure 3. Layer of icosahedra with Li and Si atoms below and above (light, bold: exohedral Si–B bonds; dark, bold: exohedral B–B bonds [Å], e.s.d. 0.001 Å).

As in $MgB_{12}Si_2$,[8] the B_{12}^{2-} units are somewhat distorted (Figure 4). They consist of four independent boron atoms with endohedral B–B bond lengths varying from 1.765(1) to 1.939(2) Å (av 1.811 Å). The distances between the only boron atoms that are not bonded to exohedral Si atoms, that is, those with exohedral B–B bonds (Figure 3), are unusually long (B4–B4 1.939(2) Å), like those found in

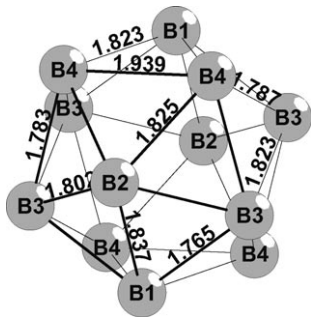

Figure 4. Endohedral bonds of a B_{12} icosahedron [Å], e.s.d. 0.001 Å.

$MgB_{12}Si_2$[8] as well. We suggest electronic reasons for this phenomenon (see below).

The silicon atoms are each bonded to four icosahedra in a distorted tetrahedral surrounding. They connect the layers of B_{12} units in such a way that three of the four icosahedra belong to one layer and the fourth one to the next layer (Figure 5). The B-Si-B angles are 100.43(4)–125.16(5)°, and

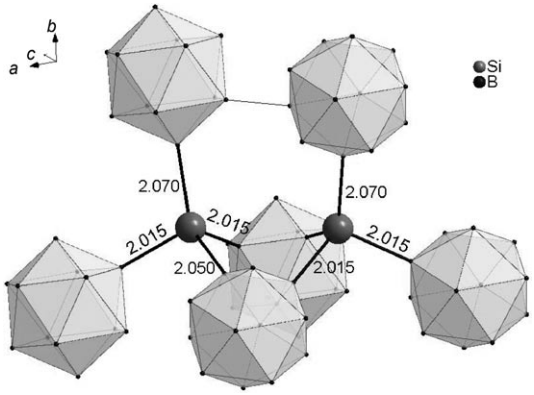

Figure 5. Coordination of Si in $Li_2B_{12}Si_2$ (bond lengths [Å], e.s.d. 0.001 Å).

the Si–B distances of 2.015(1)-2.070(1) Å (av 2.038(1) Å) are similar to those in $MgB_{12}Si_2$,[8] SiB_3[14] and $Mg_3B_{36}Si_9C$.[15] The sum of the covalent radii of Si and B is 2.05 Å, so we assume Si–B single bonds in this structure, slightly influenced by secondary orbital interactions between Si and the B_{12} units, which also cause the long endohedral B4–B4 distance (see below).

Lithium is located in voids of the covalent framework. The coordination sphere is made up by nine boron atoms, that is, one face and three edges of neighboring icosahedra, and two silicon atoms (Figure 6). The Li–B distances are between 2.313(3) and 2.609(4) Å, comparable to those in $Li_2B_{12}C_2$.[7] The Li–Si distances are 2.347(3) and 2.544(3) Å, less than 0.09 Å shorter than the Mg–Si distances in $MgB_{12}Si_2$.[8] Li is located on the mirror plane (011). The large displacement parameters of Li, caused by its low

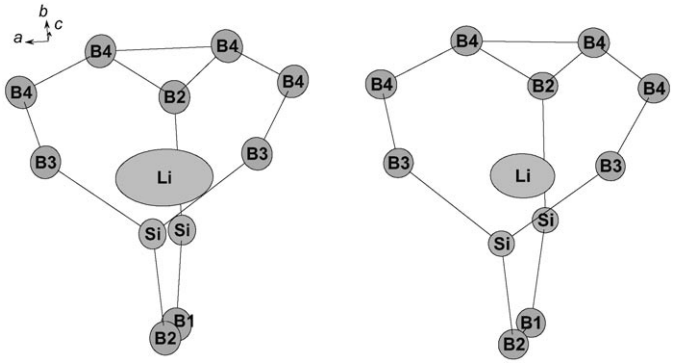

Figure 6. Surrounding of Li in $Li_2B_{12}Si_2$ (left: room temperature, right: 100 K; ellipsoids with 99% probability).

weight, show a significant anisotropy ($U_{11}/U_{33} \approx 3$). This can be interpreted as thermal motion or as a split position. A structure refinement with the Li atom on a split position about 0.02 Å from the mirror plane converges with the same R values as that with the Li atom on the mirror plane. A distinction between these two models can be drawn by means of temperature-dependent X-ray measurements. In the case of a split position the deviation from the mirror plane should increase at lower temperature. Refinement of the data collected at 100 K reveals that it is a dynamic phenomenon (Figure 6). The anisotropy of the displacement parameters is still present, but clearly reduced. The refinement with split positions is still possible, but the shift is diminished to 0.015 Å. The reduction of the displacement parameters U_{11}, U_{22}, and U_{33} at 100 K are of a magnitude which corresponds to the decrease in temperature. The anisotropic surroundings are the cause of the shape of the displacement ellipsoid, as the lithium ion has more space to move in the direction perpendicular to the mirror plane. Similar observations were made for other boron-rich borides containing Li and Mg.[16] In general the displacement parameters of Si and B are very small and uniform. This seems to be characteristic of hard materials based on a covalent framework and was also observed for related boron-rich borides.[7,8,11,12]

The similarity of $Li_2B_{12}Si_2$ and $MgB_{12}Si_2$ also spans the coordination spheres of the cations. In $MgB_{12}Si_2$ the surroundings of Mg were exactly like those of Li in this structure, and even the distances between the cation and the atoms around it are very similar.[8] The close relationship between these structures can be shown with a simple group/subgroup diagram[17] (Figure 7). Therefore, clearly the only reason for

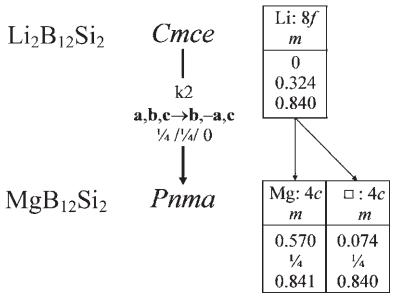

Figure 7. Group/subgroup relation of $Li_2B_{12}Si_2$ and $MgB_{12}Si_2$.

the higher symmetry of $Li_2B_{12}Si_2$ is the fact that this structure has twice as many cations as $MgB_{12}Si_2$, since the $B_{12}Si_2^{2-}$ framework gains two electrons per formula unit either from one Mg atom or from two Li atoms. Thus, reduction of symmetry from space group *Cmce* (no. 64) to *Pnma* (no. 62) occurs by splitting the Li position into the Mg position and another position that is unoccupied in $MgB_{12}Si_2$. As a side effect, the boron and silicon positions are split as well, that is, the number of symmetry-independent positions is duplicated. On the whole, the covalent framework remains the same, consistent with the fact that single crystals of both compounds are yellow and transpar-

ent. $Li_2B_{12}Si_2$ and $MgB_{12}Si_2$ are the first examples of the same electron-precise network of B_{12} icosahedra with two different metals. This is further evidence that simple electron counting rules such as those of Wade and Longuet-Higgins[9] can work in solid compounds and can even be used to explain relationships between structures.

$Li_2B_{12}Si_2$ is also related to SiB_3 ($B_{12}(Si_2)_2$),[14] in which the B_{12} units are arranged in the same type of pseudo-hexagonal layers by formation of four exohedral B–B bonds. These layers are interconnected by Si_2 units in a zigzag array. Therefore every icosahedron has four exohedral B–B bonds and eight exohedral B–Si bonds as well.

Vibrational spectra: Figures 8 and 9 show the IR and Raman spectra of $Li_2B_{12}Si_2$ and the structurally closely related compound $MgB_{12}Si_2$. As expected, the spectra are very similar, but especially the Raman spectrum of the former shows fewer signals with lower resolution. This seems to be due to the absorption properties of $Li_2B_{12}Si_2$; in the case of $MgB_{12}Si_2$ it was possible to measure Raman spectra with powder as well as with a single crystal in different orientations, but powder samples of $Li_2B_{12}Si_2$ did not provide suitable spectra even when different wavelengths (514.5 nm, 647.1 nm, 676.4, 1063 nm) were used. The possibility of decomposition of the compound by laser radiation was excluded.

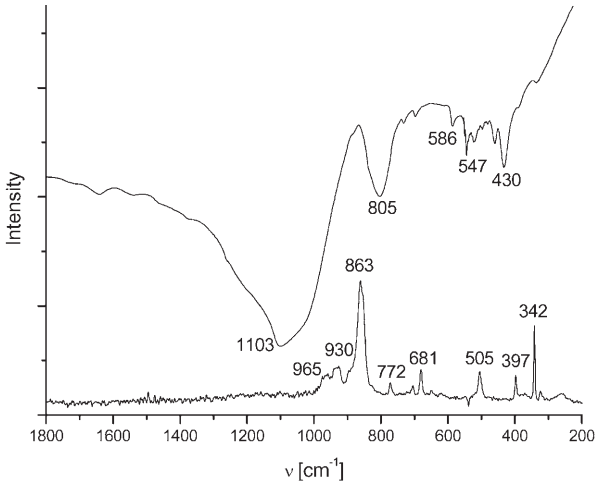

Figure 8. IR (top) and Raman spectra of $Li_2B_{12}Si_2$ (some weak Bands are not labeled, see Tables 1 and 2).

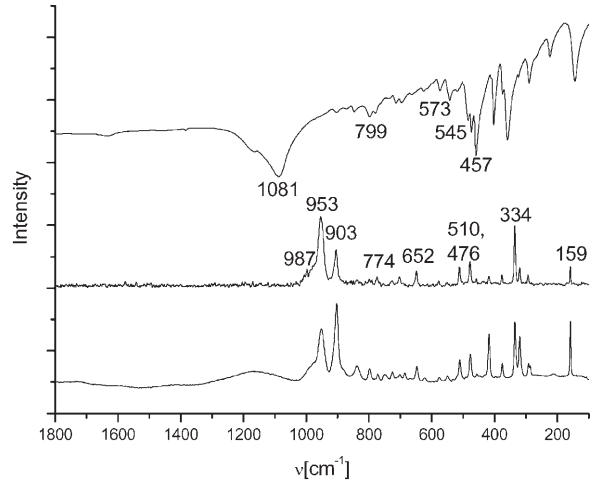

Figure 9. IR and Raman spectra of $MgB_{12}Si_2$: Top: IR spectrum, middle: Raman spectrum obtained from a single crystal, bottom: Raman spectrum obtained from powder.

Spectra from single crystals were only obtained on irradiation parallel to the [001] direction. The reason for this is still ambiguous, but the crystals show high optical anisotropy: they are transparent and yellow (Figure 1) only in the [001] direction. The vibrational spectra of $Li_2B_{12}Si_2$ are therefore discussed only in a qualitative manner. A detailed assignment of modes was carried out for $MgB_{12}Si_2$, with a correlation of modes resulting from a complete factor group analysis, with polarized Raman spectra and force-field calculations as basis.[16] In addition, data for $Li_2B_{12}C_2$ and $LiB_{13}C_2$, for which force-field calculations were also performed, are taken into consideration.[16]

Comparing the spectra of $Li_2B_{12}Si_2$ in Figure 8 with published data revealed that α-rhombohedral boron and boron-rich borides exhibit bands up to 1200 cm^{-1}. The vibrations observed for $Li_2B_{12}Si_2$ and $MgB_{12}Si_2$ can be distinguished by means of reference systems such as $B_{12}H_{12}^{2-}$ for "free icosahedra", α-rhombohedral boron for the three-dimensional framework and B_4C (or $B_{13}C_2$) and related phases (i.e., $B_{12}P_2$, $B_{12}As_2$) to account for the additional influence of the non-boron atoms.

On the basis of $B_{12}H_{12}^{2-}$ and α-rhombohedral boron one can distinguish between inter- and intra-icosahedral bands.[18–20] By analogous spectroscopic investigations on boron-rich compounds with the composition $B_{12}X_2$ (X = Si, P, As) the bands of the icosahedron–X bonds are expected to occur between 200 and 600 cm^{-1}.[20–22] Overall, we must consider strong coupling of the modes resulting from the exohedral two-center bonds between the B_{12} icosahedra and the strongly covalent Si–B bonds. In fact the "free-icosahedra" ($B_{12}H_{12}^{2-}$) model is only a simplistic rough approximation. Moreover the change to the solid state causes a splitting of bands because degeneracy is broken. Both effects were supported by spectroscopic analysis of $MgB_{12}Si_2$, $Li_2B_{12}C_2$, and $LiB_{13}C_2$.[7,8]

In the range of 100 and 200 cm^{-1} librational modes are documented for α-rhombohedral boron,[18,20] which were also observed for $MgB_{12}Si_2$.

According to this factor group analysis, the description of the modes refers to the free icosahedron $B_{12}H_{12}^{2-}$ with I_h symmetry and to the rhombohedral crystal structure in α-rhombohedral boron. To keep this discussion concise, the explicit assignment of modes for $Li_2B_{12}Si_2$ and $MgB_{12}Si_2$ is not mentioned here.

Modes which appear in the range 800–1100 cm^{-1} are primarily determined by intra-icosahedral vibrations. Intra-icosahedral deformation modes can also appear at lower frequencies. Comparing the Raman spectra of $MgB_{12}Si_2$ with

that of $Li_2B_{12}Si_2$ shows that the apparent discrepancy in intensity in the group of intra-icosahedral modes is attributable to the effects of polarization.

Endohedral bond lengths of the reference systems and the Li and Mg boride silicides can be roughly correlated with the observed vibrational frequencies (Table 1). The average endohedral B–B distance in $Li_2B_{12}Si_2$ of 1.844 Å ($MgB_{12}Si_2$: 1.842 Å) is significantly longer than those in $B_{12}H_{12}^{2-}$ and α-rhombohedral boron. For $MgB_{12}Si_2$ at least, this is associated with a decrease in both ν_1(intra) and ν_2(intra), whereas ν_2-(intra) could not be observed for $Li_2B_{12}Si_2$.

Table 1. Endohedral bond lengths and predominant intra-icosahedral vibrations.

	$B_{12}H_{12}^{2-}$[19,22]		α-rhomb. B		$Li_2B_{12}Si_2$		$MgB_{12}Si_2$	
d_{endo}(B–B) [Å]	1.75		1.73–1.79		1.77–1.79; 1.80–1.825; 1.94		1.75–1.77; 1.80–1.83; 1.95	
	IR	Raman	IR[20,22]	Raman[19,23,24]	IR	Raman	IR	Raman
ν_1(intra) [cm^{-1}]	1070 (F_{1u})	949 (A_{1g})	805	933 (A_{1g})	805	861	799	903
ν_2(intra) [cm^{-1}]	720 (F_{1u})	584, 770 (H_g)	705	587, 872 (E_g)	586–430	–	573–353	575

Modes which appear at higher frequencies (900–1250 cm^{-1}) are primarily determined by exohedral B–B bonds. The increase in frequencies of intra-icosahedral modes in general can be explained by the changeover from 2e–3c bonds to 2e–2c bonds. In the case of $Li_2B_{12}Si_2$ and $MgB_{12}Si_2$ intercalation of silicon leads to strong covalent 2e–2c B–Si bonds between the B_{12} layers.

In the same way as for the intra-icosahedral vibrational bands (Table 1), qualitative assignment of the modes was possible (Table 2). Based on the Raman spectra of $B_{12}H_{12}^{2-}$, certain bands are well-defined as inter-icosahedral modes because they are associated with B–H vibrations.[23] In the range 200–600 cm^{-1} one finds deformation modes of the icosahedra as well as exohedral vibrations in which Si atoms are expected to be involved. The strong influence of vibrational coupling is shown by the significant differences between the spectra of α-rhombohedral boron and boron-rich compounds.

Hardness: Because of the strong covalent bonds within the three-dimensional network, $Li_2B_{12}Si_2$ was expected to be a hard material. This was confirmed by measurements of the microhardness (maximum load: 2 N, see Experimental Section). Vickers and Knoop values of 20.3 (H_V) and 20.4 GPa (H_K) were obtained. These values are comparable to those of other boron-rich borides. Because microhardness values depend on the measurement conditions (load, indentation time) we investigated α-AlB_{12}, too, and found slightly higher values (H_V=25.4, H_K=25.2 GPa). In an earlier investigation of *m*-$MgB_{12}C_2$[11] with a maximum load of 5 N we found nearly equal microhardness H_V for the boron-rich borides *m*-$MgB_{12}C_2$ (26–34 GPa) and B_4C (27–30 GPa). Published values for α-AlB_{12} and $B_{48}Al_3C_2$, are 25.3[25] and 30 GPa,[26] respectively. These values are higher than that of Al_2O_3 (21 GPa[27]) and lower than those of c-BN (45 GPa[27]) and diamond (100 GPa[27]). The microhardness of $Li_2B_{12}Si_2$ is similar to that of Al_2O_3. Probably, the lower microhardness of $Li_2B_{12}Si_2$ results from the higher content of Li^+ cations, which do not contribute to the covalent network and thus lower the microhardness.

UV/VIS data: Figure 10 shows the UV/Vis spectrum of $Li_2B_{12}Si_2$. The absorbance has no maxima within the whole detection range (200–800 nm) but changes significantly between 550 and 500 nm. This is typical for a semiconductor/isolator in which the optical properties are determined by an optical band gap. The onset of the absorption edge can be determined by linear regression. For $Li_2B_{12}Si_2$ a value of 546.6 nm (2.27 eV) was obtained.

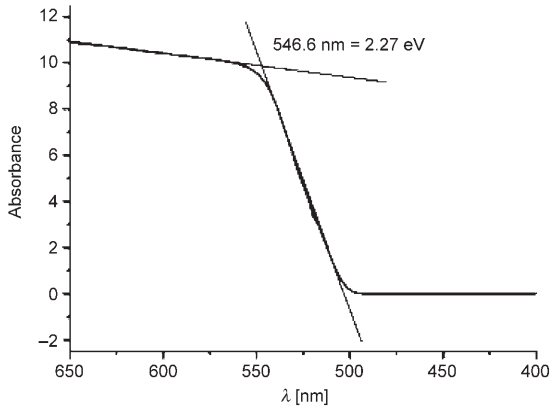

Figure 10. UV/Vis spectrum of $Li_2B_{12}Si_2$.

Table 2. Exohedral bond lengths and predominant inter-icosahedral vibrations.

	α-rhomb. B[23,24]		$Li_2B_{12}Si_2$		$MgB_{12}Si_2$	
d_{exo1} [Å] (2c–2e bonding)	1.71		1.795		1.78	
d_{exo2} [Å]	2.02 (3c–2e bonding)		2.01–2.07 (B–Si)		1.98–2.15 (B–Si)	
	IR	Raman	IR	Raman	IR	Raman
ν_1(inter) [cm^{-1}]	1202, 1234	1186 (A_{1g})		965, 930		987, 953
ν_2(inter) [cm^{-1}]	1103 (E_u)	1123, 710, 776, (E_g)	1103	705, 772	1081	701, 774
ν_3(inter) [cm^{-1}]	928 (A_{2u})			258–505		216–510

Electronic structure

DOS/band structure: Band-structure calculations and the density of states (DOS) for $Li_2B_{12}Si_2$ (Figure 11) show a band gap of 2.1 eV. This is in good agreement with the experimentally acquired band gap from UV/Vis measure-

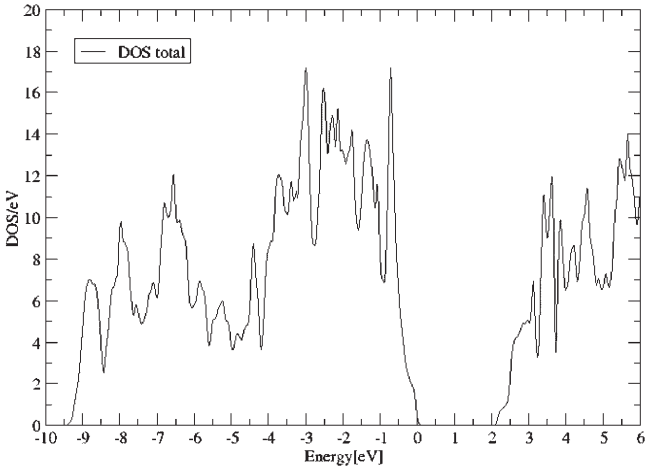

Figure 11. Calculated TDOS of $Li_2B_{12}Si_2$.

ments of 2.27 eV (Figure 10). The band structure (Figure 12) of $Li_2B_{12}Si_2$ shows that the compound is a direct Γ-point semiconductor (to improve clarity the Fermi level has been increased to 0.05 eV).

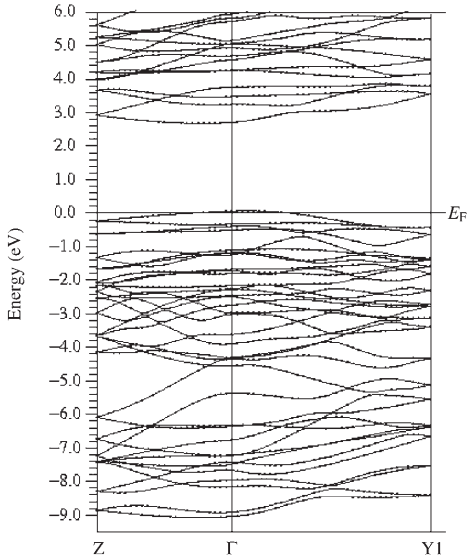

Figure 12. Band structure of $Li_2B_{12}Si_2$.

The DOS and band structure of $Li_2B_{12}Si_2$ consist of core and valence states. Here we only discuss valence states. Therefore, states below −10 eV are in general not displayed (Li 1s; B 1s; Si 1s, 2s, 2p). As a result, there are 44 bands representing 88 electrons from −9.05 eV to the Fermi level E_F. These electrons belong to the B 2s, 2p and Si 3s, 3p states; the Li atoms transfer their electrons completely to the covalent framework.

Structure and interpretation of DOS and band structure: The states near E_F are mainly dominated by p states of boron and silicon. Between −4 and −10 eV the influence of s states on both elements increases. Corresponding to the covalent bonding in the 3D framework, the DOS shows sharp peaks, while the band structure shows narrow dispersions in the range containing the p states.

Si PDOS/BS: The partial density of states (PDOS) of silicon (Figure 13) shows relatively good s–p separation, whereby

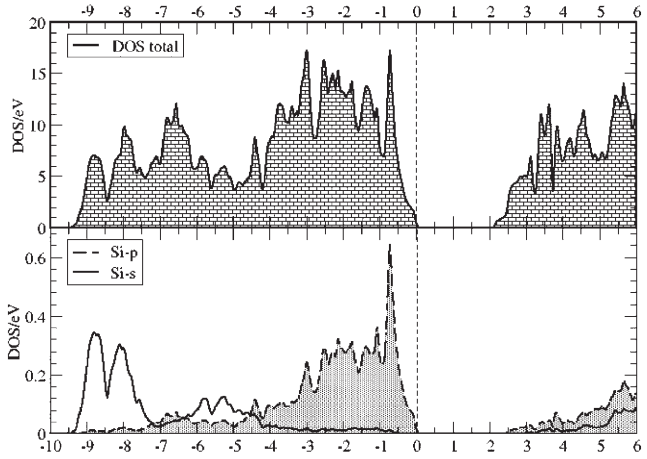

Figure 13. Si PDOS in comparison with TDOS. Overlap of Si s and Si p states is significant only between −4 and −7 eV.

the Si s states are much more delocalized than the Si p states. This suggests less pronounced sp^3 hybridization. This is also supported by the B-Si-B angles, which differ significantly from the ideal tetrahedral angle. A "fat-band" plot of the band structure reveals the valence band to have highly pronounced Si p_x character (Figure 14).

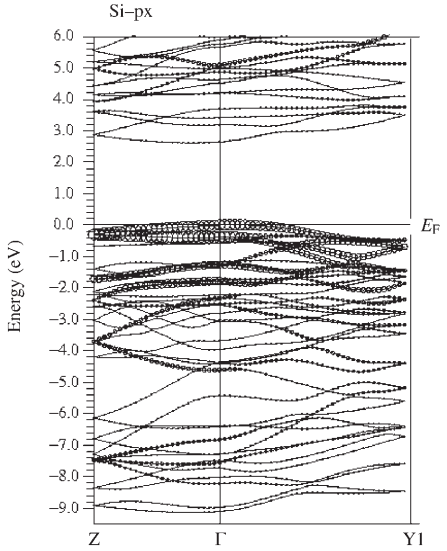

Figure 14. "Fat-band" plot of Si p_x states. The valence band decreases from Γ.

B-PDOS/BS: The PDOS of the four distinguishable B atoms (given for B3 as an example in Figure 15) shows a mixture of s and p states. According to the PDOS of the Si atoms this can be interpreted as almost total hybridization

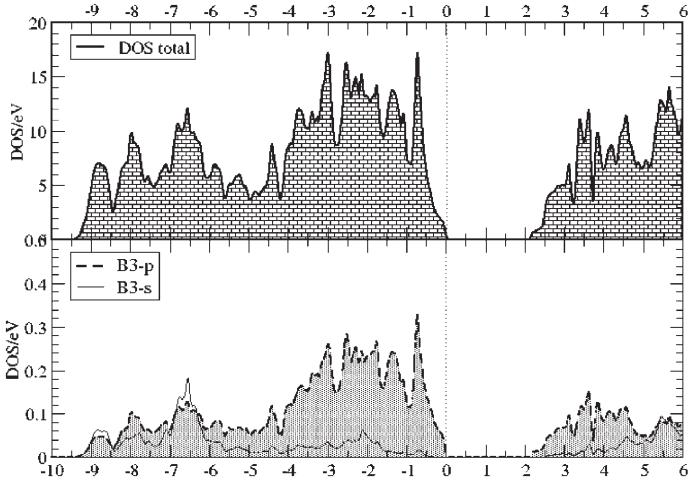

Figure 15. B3 PDOS compared to TDOS. There is total overlap between the B3 s and p states.

of the B atoms. The p states of all B atoms dominate at E_F, whereas between 0 and 0.5 eV the B3 states are most present (Figure 16). The p_x states of the B3 atoms in particular contribute to the valence band, which is also shown as a "fat-band" plot (Figure 17).

Si and B3 DOS/BS: Si–B bonds and bonding: At E_F B3 p_x states are present as well as Si p_x states, which means that the nature of the valence band is predominantly determined by both of these states (Figure 14, Figure 17, Figure 18).

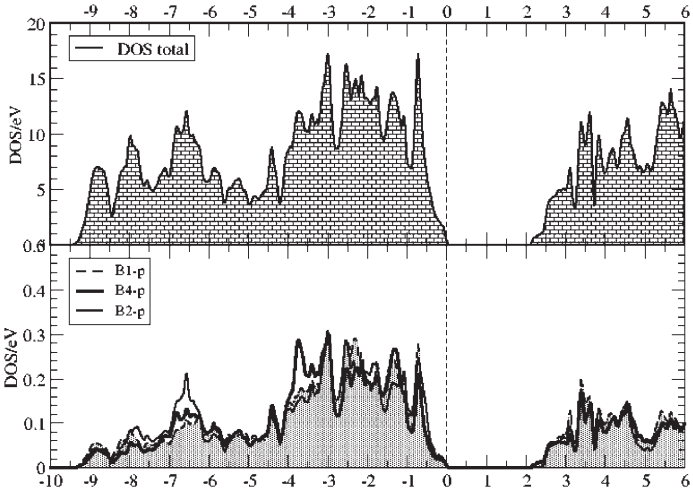

Figure 16. B-PDOS of the B atoms other than B3 in comparison with TDOS. The presence of B p states between 0 and 0.5 eV is significantly less than in the case of the B3 p states shown in Figure 15.

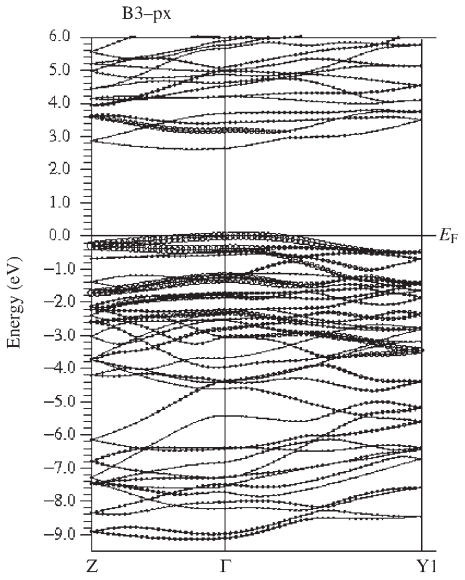

Figure 17. "Fat-band" plot of the B3 p_x states.

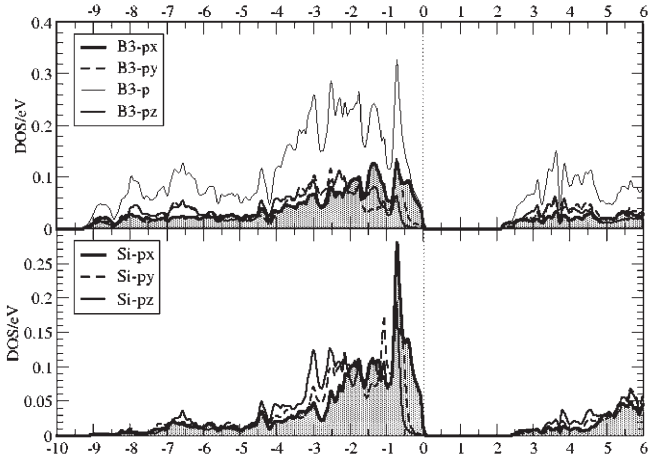

Figure 18. Si PDOS in comparison to B3-PDOS. The p_x states of B3 and Si dominate at E_F.

In the case of $Li_2B_{12}Si_2$ it is almost impossible to derive the bonding situation by interpretation of the band structure, because the 3D covalent framework produces a complex crystal structure. As a consequence of strong electronic mixing of the states of all B and Si atoms we cannot get any exact information about the Si–B bonds in general. Fortunately, we can estimate the nature of the Si–B3 bond on the basis of the Si p_x and B3 p_x fat-band plots: this bond is partly "visible" in the valence band. For this reason it is necessary to plot k paths along k_z (Z→Γ) and k_x (Γ→Y1) inside the first Brillouin zone. The Si–B3 bond is partly located in the *ac* layer. As a result the valence band shows a quite narrow dispersion (Γ→Y1) in direction of k_x or *a*. Although the dispersion is very narrow, there is a decreasing progression of the band from Γ along k_x, which means that it is σ-bonding in nature. In fact this band can be interpreted as an Si–B3 σ band or a p–p σ bond.

Icosahedron bonds: In the *ac* layer the B_{12} icosahedra are tilted and B4 atoms form the inter-icosahedral bonds inside the icosahedral layers of the framework. A B_{12} icosahedron provides 48 atomic orbitals. Twelve (radial) sp hybrid orbitals that point towards the inside of the icosahedron are disposed for exo σ bonds. The remaining 24 tangential p orbitals can form 3c bonds.[28] In this case, band-structure calculations cannot provide an absolute differentiation between intra- and inter-icosahedral bonds because of the strong mixing of all symmetry-allowed intra-icosahedral exo and endo states. Because of this we cannot classify states into radial and/or tangential bands.[6] To obtain more details of endo B–B bonds and bonding on the basis of B–B bond distances, the theoretical valence charge density can reveal much more about the electronic structure of the covalent boron framework in $Li_2B_{12}Si_2$.

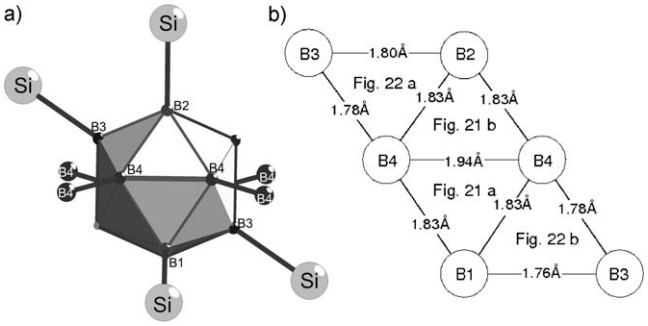

Figure 20. a) B_{12} unit and surroundings. b) Neighboring icosahedral triangles and bond lengths [Å].

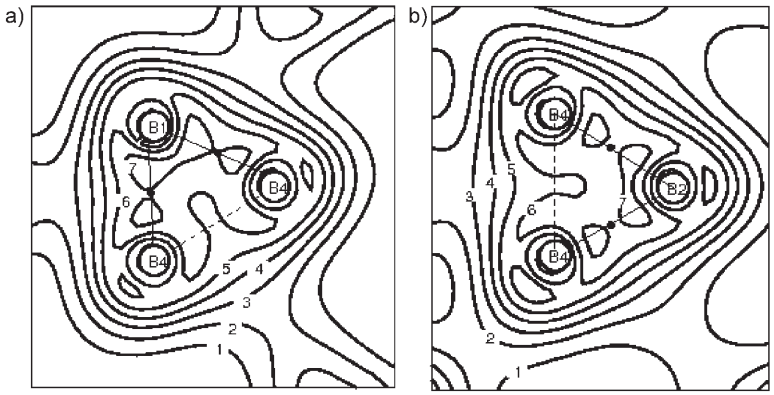

Figure 21. a, b) Neighboring icosahedral triangles. Compared to the other B–B bonds in this compound, charge density is significantly lower in the region of the very long B4–B4 bond. Solid lines represent paths containing saddle points; BCPs are marked with closed circles.

Li PDOS: electron transfer: The Li PDOS (Figure 19) shows very low density of states below E_F. The Bader method[29] gives a charge of $Li^{0.87+}$, which can be understood approximately as complete charge transfer from the Li atoms to the covalent framework of the boride.

Valence charge density ρ_{val}: Due to the variation of intra-icosahedral B–B distances it is reasonable to deal with ρ_{val} at the bond critical points (BCPs). To visualize the bonding situation in the entire icosahedron, ρ_{val} was determined for four neighboring icosahedral-triangle segments (Figure 20). Contour lines from 1 to 8 are related to a charge density of $1 = 0.14\,e\,A^{-3}$.

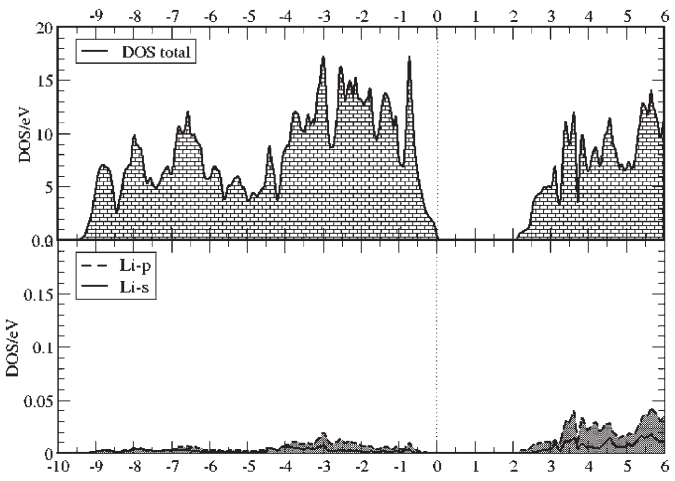

Figure 19. TDOS of $Li_2B_{12}Si_2$ in comparison to Li PDOS.

3c bonding: Figure 21 shows triangles containing the longest intra-icosahedral bonds (1.83 and 1.94 Å). Because of the lengthened B4–B4 bond (1.94 Å) the charge density in the region of the B4–B4 bond axis is lower than expected within a conventional 3c bond.[28] This shows that an electronic deformation exists within the icosahedral triangle. The positions of BCPs could only be estimated with the topology of the charge density inside regions containing B1–B4 and B2–B4 bonds (1.83 Å), where definite saddle points are indicated. From this estimation we find that $\rho_{val}^{BCP} = 0.72\,e\,Å^{-3}$ and, in the case of the B4–B4 interaction, $\rho_{val}^{BCP} = 0.62\,e\,Å^{-3}$. No BCP could be found between the B4 atoms, but there correlation with bond order is of course problematic.

Figure 22 shows icosahedral triangles located next to the triangles in Figure 21, which contain shorter B–B bonds (1.76–1.80 Å). As expected, the homogeneous charge density distribution in Figure 22a represents a conventional 3c–2e bond.[30] For these bonds saddle points were found[29] with $\rho_{val}^{BCP} = 0.73$–$0.78\,e\,Å^{-3}$. In the region of the B1–B3 bond (1.76 Å) the highest charge density of $\rho_{val}^{BCP} = 0.81\,e\,Å^{-3}$ was found, in accordance with the shortest intra-icosahedral bond length (Figure 22b).

To visualize the bonding situation within the B_{12} layers, the electronic conditions of B4–B4 exo bonds (1.795 Å) must be examined for electronic deformation: Figure 23a

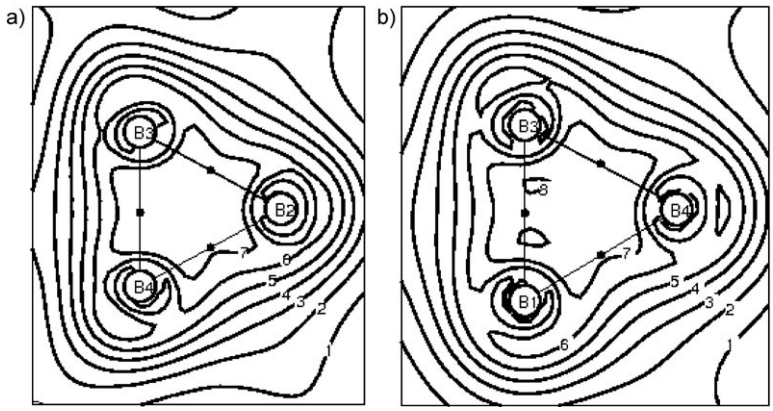

Figure 22. a) Icosahedral triangle containing bonds between 1.78 and 1.80 Å and homogenous charge density distribution. b) Icosahedral triangle containing the shortest intra-icosahedral bond (1.76 Å). Thick lines represent bonds shorter than 1.80 Å.

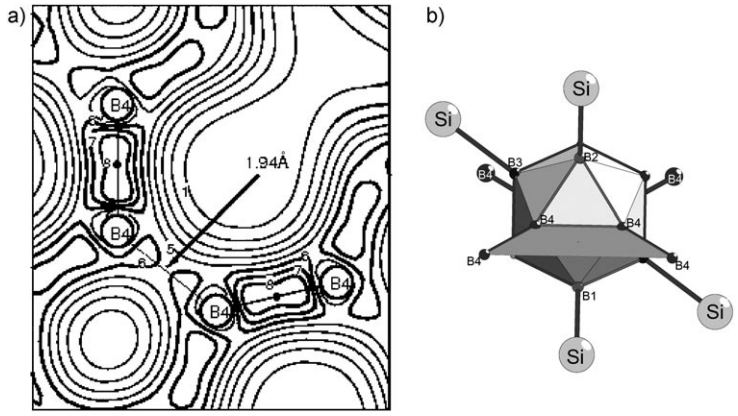

Figure 23. a) Valence charge distribution in the region of the *exo* B4–B4 bond between the B_{12} layers. b) B_{12} unit with plane showing *exo* B4–B4 bond.

shows quite localized valence charge distribution in the region of the B4–B4 exo bond axis, whereas this distribution is typical for a 2c-2e bond. Here the ρ_{val}^{BCP} value of 0.82 e Å^{-3} differs considerably from the endo B4–B4 interaction mentioned above.

Lowering of the symmetry of the B_{12} units in the rhombohedral lattice results in variation in the intra-icosahedral bond lengths and electronic deformation. However, in the case of $Li_2B_{12}Si_2$, the reason for one significantly lengthened intra-icosahedral bond, the B atoms of which are exclusively B-bonded, is still unknown. In this context, the interaction of the B4–B4 bond with the Si orbitals (Figure 24) could be discussed, although the Si atom is relatively far away (3.09 Å between the B4–B4 bond and the Si atom). The valence charge density in the region defined above shows a T-shaped pattern hinting at electrostatic interaction or partial charge transfer between the B4–B4 bond and the Si atom.

Quantum chemical investigations of compounds with similar structural and electronic properties to $MgB_{12}Si_2$[8] and SiB_3[14] are currently in progress to interpret the nature of this interaction, because the reason for the observed intra-icosahedral bond lengthening in these compounds cannot yet be finally determined. Experimental determination of valence charge density can also provide information about any interaction.

To investigate the 3D shape of the charge density it is important to visualize it perpendicular to the plane shown in Figure 25 a.[29] Perpendicular to the Si–B1 bond axis we observe a maximum in density in accordance with the existence of a saddle point. In contrast, the region of the B4-B4-Si interaction contains neither a charge density maximum nor a BCP, although charge density distribution is significant.

A possible reason for lengthening of the B4–B4 bond could be a donor–acceptor interaction in which the B4–B4

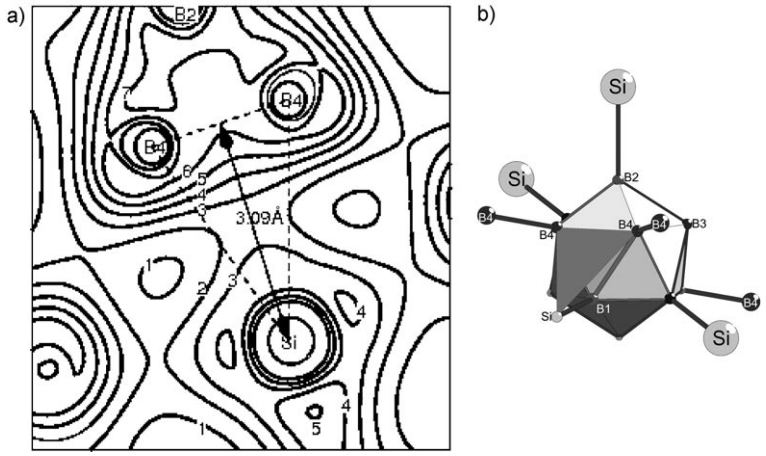

Figure 24. a) Valence charge distribution in the B4-B4-Si plane, provided as an aid to visualizing the interaction. Charge density between the bond and the Si atom is T-shaped. b) B_{12} unit with plane showing *endo* B4–B4 bond and Si atom.

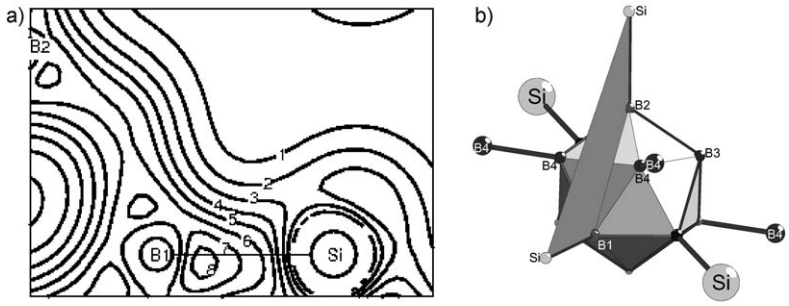

Figure 25. a) Charge density distribution perpendicular to the plane shown in Figure 24. From the Si–B1 bond, charge density decreases continuously. b) B_{12} unit with plane perpendicular to that shown in Figure 24.

bond acts as donor. Charge should thus be transferred from bonding icosahedron orbitals into antibonding acceptor orbitals of the Si atom. As a result the bond order of the *endo* B4–B4 bond would decrease. Another means of decreasing B4–B4 bond order and lengthening the bond is transfer of charge from Si atom orbitals into the B4–B4 bond in a similar way to back-donation, whereby antibonding states are populated. However, without detailed knowledge of the symmetry of the orbitals involved it is not possible to assign any donor or acceptor functions. Another noteworthy point is the absence of a BCP, which could indicate a bond path along the T-shaped distribution as evidence for any charge transfer or interaction causing an unusually long bond.

Conclusion

Single crystals of $Li_2B_{12}Si_2$ are formed from the elements in a Sn melt at 1500 °C. The crystal structure is based on B_{12} icosahedra that are connected by exohedral 2e–2c B–B bonds into layers and by Si atoms into a three-dimensional net. The transparent, yellow crystals are stable against water, air, and concentrated hydrochloric acid.

$Li_2B_{12}Si_2$ is another demonstration that the auxiliary-metal technique is a versatile tool for the synthesis and crystal growth of boron-rich borides. Under these conditions there is a strong tendency to form stoichiometric compounds with well-ordered crystal structures, in contrast to many other boron-rich borides formed by conventional HT syntheses. This has been shown before with compounds such as $Li_2B_{12}C_2$, $LiB_{13}C_2$, $MgB_{12}Si_2$, $Mg_2B_{24}C$ and $MgB_{12}C_2$. In all of these cases structural features conform to the simple electron-counting rules of Wade and Longuet-Higgins for *closo* polyhedra.

For $Li_2B_{12}Si_2$ we were able to measure a number of physical properties and to align them with band structure calculations. All of these investigations confirm that this unique class of boron-rich borides are stoichiometric and electron-precise compounds of high chemical, mechanical and thermal stability. The results are important for the search for new hard and superhard materials. Further experiments on NMR properties and experimental electron density determinations are in progress.

In the versatile structural principle of combining B_{12} icosahedra and small building units of other light main group elements like isolated atoms (B in MgB_7,[13] C in *m*-$MgB_{12}C_2$[11] and $Mg_2B_{24}C$,[12a] Si in $Li_2B_{12}Si_2$ and $MgB_{12}Si_2$,[8] C_2 in *o*-$MgB_{12}C_2$[11] and $Li_2B_{12}C_2$,[7] CBC in $LiB_{13}C_2$,[7] Si_8 and SiC in $B_{36}Si_9C$[15]), the electrons for stabilization of the B_{12} icosahedra are supplied by Li or $Mg_3B_{36}Si_9C$ cations located in voids of the covalently bonded anionic network. By variation of the experimental conditions we expect to synthesize further representatives of this special class of compounds which shows a unique combination of chemical, physical and structural properties.

Experimental Section

Synthesis: Single crystals of $Li_2B_{12}Si_2$ were synthesized from the elements in a Sn/Si melt. Sn (shots, ca. 3 mm diameter, 99.9%, ABCR), Si (lumps, 0.1–2.5 cm, 99.9999%, Alfa Aesar), Li (rod, 99%, Riedel de Haën) and B (pieces, crystalline, grade K2, ABCR) were weighed into an h-BN crucible in a molar ratio between 1:1:1:0.25 and 1:1:1:1 (total 1.5–8.8 g). The crucible was closed with an h-BN screw cap and put into a tantalum ampoule, which was sealed by arc welding. The ampoule was put into a high-temperature laboratory furnace (type LHTG, GERO Hochtemperaturöfen GmbH&Co.KG) and heated in an argon atmosphere up to 1500 °C, held for 40 h and cooled to room temperature at 60 °C h^{-1}. The ampoule was opened and Sn was removed by dissolution in conc. HCl for several hours. Single crystals of $Li_2B_{12}Si_2$ are yellow, transparent and mostly shaped like polyhedra with sizes up to 1.5 mm. There was no by-product except for single crystals of silicon.

Elemental analysis: Qualitative and quantitative analyses on several single crystals of $Li_2B_{12}Si_2$ were made by EDX and WDX measurements. The samples were fixed with conducting glue on a graphite platelet mounted on an aluminium sample holder. Besides the presence of Si and B it was confirmed that no other element heavier than B was present. The EDX (REM: DSM 962, Carl Zeiss; EDX device: INCA Energy 300, Oxford) analysis with B and SiO_2 as standards showed molar B/Si ratios of 85.4:14.1 (±0.4) on average. WDX (Cameca SX100) measurements with the standard $MgB_{12}Si_2$ yielded B/Si/X = 74.8:12.6:12.6 (calcd 12.5:75.0:12.5). The value of X was measured by difference and matches the expected percentage of Li perfectly, as no other elements with $Z > 4$ were found.

Crystal structure determination: Diffraction data for single crystals of $Li_2B_{12}Si_2$ were measured with an Image Plate Diffraction System (IPDS II, Stoe) with $Mo_{K\alpha}$ radiation. Several single crystals of different batches were measured. A *C*-centered orthorhombic cell with $a = 6.1060(6)$, $b = 10.9794(14)$, and $c = 8.4050(8)$ Å was found. Details of the best refinement are listed in Table 3. Because of the low absorption coefficient (0.5 mm^{-1}), no absorption correction was done. Structure solution with direct methods (SHELXTL[31]) in *Cmce* gave a structure model with six independent atoms. The elements were assigned according to electron densities and distances between atoms. All atoms were refined with anisotropic displacement parameters. Every occupation factor was refined separately as a free variable within very small standard deviations. Full occupation was observed for every atom. 582 reflections and 44 parameters resulted in *R* values of $R_1(F) = 0.0249$ and $wR_2(I) = 0.0631$. Atom coordinates and displacement parameters are listed in Tables 4 and 5. Se-

Table 3. Crystallographic data and structure refinement for $Li_2B_{12}Si_2$.

T [K]	293(2)
crystal shape	regular polyhedron
color	yellow transparent
crystal size [mm]	$0.1\times0.1\times0.1$
crystal system	orthorhombic
space group	*Cmce* (no. 64)
a [Å]	6.1060(6)
b [Å]	10.9794(14)
c [Å]	8.4050(8)
V [Å^3]	563.47(11)
Z	4
ρ_{calcd} [g cm^{-3}]	2.355
data collection[a]	STOE IPDS II, $0°\le\omega\le180$, $\psi=0$, 111, $\Delta\omega=1°$
exposure time [s]	120
theta range	$3<2\theta<71°$, $-9<h<9$, $-17<k<17$, $-13<l<11$
μ [mm^{-1}]	0.50
absorption correction	none
R_{int}; R_σ	0.140; 0.050
refinement	SHELXTL,[31] full-matrix least-squares refinement on F^2
$N(hkl)$ measured; unique	8527; 653
$N'(hkl)$ $(I>2\sigma I)$	582
parameters refined	44
R_1; wR_2	0.0249; 0.0631
all-data R_1	0.0316
weighting scheme[31]	0.0207; 0.1332
extinction correction[31]	0.123(10)
GoF	1.098
residual electron density [e Å^{-3}]	max. +0.33, min. −0.29, $\sigma=0.07$

[a] $Mo_{K\alpha}$ ($\lambda=0.71073$ Å), graphite monochromator.

Table 4. Atom coordinates, site occupation factors, isotropic displacement parameters [Å^2] of $Li_2B_{12}Si_2$.

Atom	Site	x	y	z	S.O.F.[a]	U_{eq}
Si	8f/m	0.0	0.33471(3)	0.11963(4)	0.964(4)	0.0044(1)
Li	8f/m	0.0	0.3235(3)	0.8407(4)	0.94(2)	0.0258(8)
B1	8f/m	0.0	0.3994(1)	0.3485(2)	1.04(1)	0.0053(2)
B2	8f/m	0.0	0.1525(1)	0.0563(2)	1.03(1)	0.0055(2)
B3	16g	0.2654(2)	0.4207(1)	0.0319(1)	1.00(1)	0.0052(2)
B4	16g	0.3413(2)	0.5395(1)	0.1663(1)	1.00(1)	0.0052(2)

[a] To check for mixed occupations and/or vacancies, site occupation factors were treated by turns as free variables at the end of the refinement.

Table 5. Anisotropic displacement parameters [Å^2] of $Li_2B_{12}Si_2$.

Atom	U_{11}	U_{22}	U_{33}	U_{12}	U_{13}	U_{23}
Si	0.0039(2)	0.0047(2)	0.0048(2)	0.0001(1)	0	0
Li	0.049(2)	0.018(1)	0.011(1)	0.000(1)	0	0
B1	0.0047(5)	0.0060(4)	0.0051(5)	0.0002(4)	0	0
B2	0.0049(5)	0.0058(5)	0.0058(6)	0.0001(4)	0	0
B3	0.0047(3)	0.0055(3)	0.0053(4)	0.0002(3)	0.0000(3)	0.0002(3)
B4	0.0049(3)	0.0056(3)	0.0051(4)	0.0001(3)	0.0002(3)	0.0005(2)

lected distances and angles are listed in Table 6. Further details on the crystal structure investigations may be obtained from the Fachinformationszentrum Karlsruhe, 76344 Eggenstein-Leopoldshafen, Germany (fax: (+49) 7247-808-666; e-mail: crysdata@fiz-karlsruhe.de), on quoting the depository number CSD-418627.

Table 6. Selected distances [Å] and angles [°].

Si−B1	2.050(1)	Li−B4	$2\times2.313(3)$
Si−B2	2.070(1)	Li−B4	$2\times2.570(2)$
Si−B3	$2\times2.015(1)$	B1−B2	1.837(2)
B1-Si-B2	125.16(5)	B1−B3	$2\times1.765(1)$
B1-Si-B3	100.43(4)	B1−B4	$2\times1.823(1)$
B2-Si-B3	111.01(3)	B2−B3	$2\times1.802(1)$
B3-Si-B3	107.08(5)	B2−B4	$2\times1.825(1)$
Li−Si	2.347(3)	B3−B3	1.823(2)
Li−Si	2.544(3)	B3−B4	1.783(1)
Li−B1	2.448(4)	B3−B4	1.787(1)
Li−B2	2.405(4)	B4−B4	1.796(2) (*exo*)
Li−B2	2.609(4)	B4−B4	1.939(2)
Li−B3	$2\times2.519(3)$	B4-B4-B4	128.37(6)

Microhardness: Microhardness was measured with a microhardness equipment MHT 10 (A. Paar, Austria). A force of 2 N was generated within 10 s and applied for 15 s. The imprints of the indenters (Vickers: square pyramid, Knoop: rhombic pyramid) were evaluated and converted to a microhardness value according to the usual procedures.[32]

IR and Raman spectra: The FTIR and FT Raman measurements were performed with a Bruker IFS66v spectrometer. The IR sample was made of crystalline powder pressed with KBr into pellets. Raman measurements were carried out with a Nd:YAG laser with an output of 100 mW and 1000 scans on single crystals with a Raman microscope. Powder samples were prepared in 0.3 mm capillaries and measured with an output of 400 mW and 5000 scans.

UV/VIS spectra: The single-crystal UV/Vis spectra were measured with a JASCO V-570 UV/VIS/NIR photometer in the range from 200 to 2500 nm.

Calculations: Calculations on $Li_2B_{12}Si_2$ were performed with the full potential linearized augmented plane wave (FP-LAPW) method. Exchange and correlation were treated within the generalized gradient approximation (GGA) in the Engel–Vosko version[33] with the WIEN2k program package. In the calculation the following muffin tin radii R_{mt} were used: Si 2.0 a.u. (106 pm), Li 1.44 a.u. (74.2 pm), B 1.66 a.u. (88 pm). Self-consistency was achieved by requiring a convergence of the total energy smaller than 10^{-5} Ry/cell and a charge distance of about 10^{-5}. The cut-off energy was $R_{mt}\cdot k_{max}=5$ unitary. Integration of the Brillouin zone to determine total and partial DOS (TDOS, PDOS) was carried out by the tetrahedron method (4000 k points/BZ; 540/IBZ) and the irreducible wedge for band structure plots along the k path ZΓY1 were calculated with a grid of 60 k points. Valence charge distribution ρ_{val} was described with the program xcrysden.[34]

Acknowledgements

We thank Dr. H. Rotter, Dr. T. Ludwig, and A. Becherer for support with the IR/Raman and UV/Vis spectra, Dr. M. Ade, Dr. H. Müller-Sigmund (University of Freiburg, Institute for Mineralogy and Geochemistry) for assistance with the WDX measurements, S. Haseloff for the EDX measurements, and Dipl. Chem. Dominik Kotzott for microhardness measurements.

[1] a) V. I. Matkovich, *Boron and Refractory Borides*, Springer, Berlin, **1977**; b) T. Lundström in *Encyclopedia of Inorganic Chemistry* (Ed.: R. B. King), Wiley, New York, **1994**.
[2] a) D. Emin, *Phys. Today* **1987**, *20*, 55; b) G. A. Samara, H. L. Tardy, E. Venturini, T. L. Aselage, D. Emin, *Phys. Rev. B* **1993**, *48*, 1468.
[3] C. Wood, *Rep. Prog. Phys.* **1988**, *51*, 459.
[4] a) R. Riedel, *Adv. Mater.* **1994**, *6*, 549–560; b) R. Telle, *Chem. unserer Zeit* **1988**, *22*, 93–99.

[5] a) D. C. Halverson, A. Pyzik, I. Aksay, *Ceram. Eng. Sci. Proc.* **1985**, *6*, 736–744; b) A. Pyzik, D. Beamon, *J. Am. Ceram. Soc.* **1995**, *78*, 305–312.
[6] M. M. Balakrishnarajan, P. D. Pancharatna, R. Hoffmann, *New J. Chem.* **2007**, *31*, 473–485.
[7] N. Vojteer, H. Hillebrecht, *Angew. Chem.* **2006**, *118*, 172–175; *Angew. Chem. Int. Ed.* **2006**, *45*, 165–168.
[8] T. Ludwig, H. Hillebrecht, *J. Solid State Chem.* **2006**, *179*, 1623–1629.
[9] a) K. Wade, *Adv. Inorg. Chem. Radiochem.* **1976**, *18*, 1; b) W. N. Lipscomb, *Adv. Inorg. Chem. Radiochem.* **1950**, *1*, 117; c) H. C. Longuet-Higgins, M. de V. Roberts, *Proc. Roy. Soc. A* **1955**, *230*, 110.
[10] a) H. Hillebrecht, F. Meyer, *Angew. Chem.* **1996**, *108*, 2655; *Angew. Chem. Int. Ed. Engl.* **1996**, *35*, 2499; b) H. Hillebrecht, M. Ade, *Angew. Chem.* **1998**, *110*, 981; *Angew. Chem. Int. Ed.* **1998**, *37*, 935; c) H. Hillebrecht, K. Gebhardt, *Angew. Chem.* **2001**, *113*, 1492; *Angew. Chem. Int. Ed.* **2001**, *40*, 1445; d) V. Adasch, K.-U. Hess, H. Hillebrecht, DE-OS 102004014315, **2005**; [*Chem. Abstr.* **2005**, 142, 413894]; e) V. Adasch, PhD thesis, University of Bayreuth, **2005**.
[11] V. Adasch, K.-U. Hess, T. Ludwig, N. Vojteer, H. Hillebrecht, *Chem. Eur. J.* **2007**, *13*, 3450–3458.
[12] a) V. Adasch, K.-U. Hess, T. Ludwig, N. Vojteer, H. Hillebrecht, *J. Solid State Chem.* **2006**, *179*, 2155–2162; b) V. Adasch, K.-U. Hess, T. Ludwig, N. Vojteer, H. Hillebrecht, *J. Solid State Chem.* **2006**, *179*, 2900–2907; c) V. Adasch, K.-U. Hess, T. Ludwig, N. Vojteer, H. Hillebrecht, *J. Solid State Chem.* **2006**, *179*, 2916–2926.
[13] A. Guette, M. Barret, R. Naslain, P. Hagenmuller, L.-E. Tergenius, T. Lundström, *J. Less-Common Met.* **1981**, *82*, 325–334.
[14] a) B. Hirsche, Symposium on Solid State Chemistry, May/June **2002**, Hirschegg, Austria; b) J. R. Salvador, D. Blic, S. D. Mahanti, M. G. Kanatzidis, *Angew. Chem.* **2003**, *115*, 1973–1976; *Angew. Chem. Int. Ed.* **2003**, *42*, 1929–1932; c) B. Hirsche, PhD Thesis, University of Bayreuth, **2005**.
[15] a) T. Ludwig, H. Hillebrecht, Proceedings 15th International Symposium on Boron, Borides and Related Materials, ISBB05, 21–26 August **2005**, Hamburg, Germany; b) T. Ludwig, H. Hillebrecht, unpublished results.
[16] H. W. Rotter, H. Vojteer, H. Hillebrecht, unpublished results.
[17] a) H. Bärnighausen, *MATCH* **1980**, *9*, 139–175; b) *International Tables for Crystallography, Vol. A1* (Eds.: H. Wondratschek, U. Müller), Kluwer Academic Press, Dordrecht, **2004**.
[18] K. Shirai, S. Emura, *J. Phys. Condens. Matter* **1996**, *8*, 10912–10929.
[19] W. Weber, M. F. Thorpe, *J. Phys. Chem. Solids* **1975**, *36*, 947–974.
[20] H. Werheit, H. Haupt, *Z. Naturforsch. A* **1987**, *42*, 925–934.
[21] D. R. Tallant, T. L. Aselage, A. N. Campbell, D. Emin, *Phys. Rev. B* **1989**, *40*, 5649–5655.
[22] H. J. Becher, F. Thévenot, *Z. Anorg. Allg. Chem.* **1974**, *410*, 274–286.
[23] N. Nogi, S. Tanaka, *J. Solid State Chem.* **2006**.
[24] K. Shirai, S. Gonda, *J. Phys. Chem. Solids* **1996**, *57*, 109–123.
[25] F. Beneshovsky in *Ullmanns Enzyklopädie der Technischen Chemie, Vol. 8*, 4th ed., VCH, Weinheim, p. 657–662.
[26] V. Gurin, L. I. Derkachenko, *Prog. Cryst. Growth Charact.* **1993**, *27*, 163–199.
[27] H. Sachdev, *Nachr. Chem. Tech. Lab.* **2003**, *51*, 911–916.
[28] M. Rohde, M. Wendorff, C. Röhr, *Z. Anorg. Allg. Chem.* **2006**, *632*, 1195–1205.
[29] R. W. F. Bader, *Atoms in Molecules. A Quantum Theory. Int. Series of Monographs on Chemistry*, Clarendon Press, Oxford, **1994**.
[30] D. Li, Y.-N. Xu, W. Y. Ching, *Phys. Rev. B* **1992**, *45*, 5895–5905.
[31] G. M. Sheldrick, SHELXTL program package, University of Göttingen, Germany, **1997**.
[32] DIN EN 6507.
[33] P. Blaha, K. Schwarz, G. K. H. Madsen, D. Kvasnicka, J. Luitz, WIEN2K-An Augmented Plane Wave and Local Orbital Program for Calculating Crystal Properties, TU Wien, **2001**.
[34] A. Kokalj, *J. Mol. Graphics* **1999**, *17*, 176.

Received: December 8, 2007
Revised: April 23, 2008
Published online: July 10, 2008

